Supporting Online Material

Calculation of synthetic MSU temperatures

We employed a static vertical weighting function to calculate synthetic satellite temperatures from model and radiosonde data. For large area averages, this approach yields decadal-timescale temperature changes similar to those obtained with a full radiative transfer code (*S1*). The static weighting function was applied to vertical profiles of monthly-mean, zonally-averaged atmospheric temperature anomalies (for radiosonde data) and to temperature profiles at individual grid-points (for model data). Results were then spatially averaged over the deep tropics (20°N-20°S).

Actual MSU temperatures

We used version 5.1 of the UAH MSU T_4, T_2, and T_{2LT} data and version 1.3 of the RSS MSU data. A T_2 product independently produced by a group at the University of Maryland (UM) shows tropospheric warming exceeding that in RSS and UAH (*S2*). The UM dataset is currently available in global mean form only, and so could not be used in our investigation of tropical temperature changes.

Estimation of T_{Fu}

This was calculated as $T_{Fu} = a\ T_2\ - b\ T_4$, with coefficients $a = 1.1$ and $b = -0.1$. We applied these coefficients to the monthly-mean, spatially-averaged (20°N-20°S) T_2 and T_4 anomalies from satellites (UAH and RSS), radiosondes (HadAT2 and RATPAC), and the IPCC historical forcing simulations. Note that a and b were derived mathematically (from the T_2 and T_4 weighting functions) rather than empirically (*S3*). Trends in T_{Fu} receive only a small contribution ($< \pm 0.005$°C/decade) from the cooling stratosphere. The peak of the broad effective weighting function for T_{Fu} occurs between *ca.* 300 and 400 hPa. The peak weight for T_{2LT} is lower in the atmosphere, between *ca.* 600 and 700 hPa (*S3*).

Calculation of temporal standard deviations

All temporal standard deviations used for the calculation of $R_S(z)$ results in Figs. 3 and 4 were estimated from linearly detrended data. This was done because some of the model simulations examined here have large decadal trends in surface and atmospheric temperature, which inflate the temporal variance of the raw T_S and $T(z)$ data. This aliasing effect makes it difficult to use standard deviations estimated from raw data to separate amplification behavior on monthly and decadal timescales.

Subsampling observed T_s data with radiosonde coverage

Subsampling surface temperature data at radiosonde locations actually degrades r, the correlation between time series of monthly-mean $T_{2\mathrm{LT}}$ and T_S anomalies. For example, $r = 0.82$ for tropical average anomalies calculated from the unsubsampled HadCRUT2v T_S data and the HadAT2 radiosonde $T_{2\mathrm{LT}}$ data. The correlation is decreased ($r = 0.73$) if the same radiosonde data are correlated with the HadCRUT2v T_S data subsampled at the radiosonde locations. This result must be related to the fact that surface temperature fluctuations have smaller correlation length scales than temperature fluctuations in the free troposphere (*S4*).

Modeling groups contributing to IPCC database

At the time this research was conducted, 19 modeling groups had performed a wide range of simulations in support of the IPCC Fourth Assessment Report. Climate data from these simulations were made available to the scientific community through the U.S. Dept. of Energy's Program for Climate Model Diagnosis and Intercomparion (PCMDI).

One of the simulations (the so-called "20c3m" run) involved historical changes in a number of anthropogenic and natural forcings. The following modeling groups provided multiple realizations of the 20c3m run (the text in parentheses gives the

official model designation): the National Center for Atmospheric Research in Boulder (CCSM3, five; PCM, four); the Max-Planck Institute for Meteorology in Germany (ECHAM5/MPI-OM, three); the Institute for Atmospheric Physics in China (FGOALS-g1.0, three), the Geophysical Fluid Dynamics Laboratory in Princeton (GFDL-CM2.0, three; GFDL-CM2.1, three), the Goddard Institute for Space Studies in New York (GISS-AOM, two; GISS-EH, five; GISS-ER, five); the Center for Climate System Research, National Institute for Environmental Studies, and Frontier Research Center for Global Change in Japan (MIROC-CGCM2.3.2(medres), three; MIROC-CGCM2.3.2(hires), one); and the Meteorological Research Institute in Japan (MRI-CGCM2.3.2, five). Individual realizations were supplied by the Canadian Centre for Climate Modelling and Analysis (CCCma-CGCM3.1(T47)); Météo-France/Centre National de Recherches Météorologiques (CNRM-CM3); the Institute for Numerical Mathematics in Russia (INM-CM3.0); the Institute Pierre Simon Laplace in France (IPSL-CM4); and the Hadley Centre for Climate Prediction and Research in the U.K. (UKMO-HadCM3 and UKMO-HadGEM1). Some groups provided results for several different model configurations.

Forcings used in 20c3m runs

Details of the natural and anthropogenic forcings used by differing modeling groups in their IPCC "historical forcing" simulations are given in Table 1. This Table was com-

piled using information that participating modeling centers provided to the PCMDI (see http://www-pcmdi.llnl.gov/ipcc/model_documentation). Model acronyms are defined in the previous section.

A total of 11 different forcings are listed in Table 1. A letter 'Y' denotes inclusion of a specific forcing. As used here, 'inclusion' signifies the specification of time-varying forcings, with changes on interannual and longer timescales. Forcings that were varied over the seasonal cycle only, or not at all, are identified with a dash. A question mark indicates a case where there is uncertainty regarding inclusion of the forcing.

Stratification of 20c3m simulations

In Fig. 3, simulations were stratified according to model groups that included both stratospheric ozone depletion and volcanic aerosols (O+V) and groups that omitted these forcings. Only 9 (12) of the 19 IPCC models included forcing by volcanic aerosols (stratospheric ozone). There is no indication that the $R_S(z)$ results in Fig. 3A reflect this stratification. However, some of the largest $R_\beta(z)$ values in the lower troposphere occur in realizations performed with CCSM3, GFDL-CM2.1, and GISS-EH (Fig. 3B). All three of these models included changes in carbonaceous aerosols, which may act to warm the lower troposphere relative to the surface, thus increasing $R_\beta(z)$ (*S5*).

Simulated and observed changes in T_4

The overall stratospheric cooling during the satellite era is related to stratospheric ozone depletion (*S6*). The warming of T_4 after the eruptions of El Chichón in April 1982 and Pinatubo in June 1991 is due to the absorption of incoming solar radiation and upwelling terrestrial radiation by volcanic aerosols (*S6*, *S7*). A change in the phase of the QBO during the Pinatubo eruption induced cooling of the equatorial stratosphere (*S8*), thus damping the stratospheric warming response to Pinatubo. QBO variability is not well-simulated by most models in the IPCC archive, which partly explains why the simulated T_4 response to Pinatubo is larger and less attenuated in the model simulations.

Anomalous $R_\beta(z)$ results

Two of the 49 model realizations (INM-CM3.0) and (ECHAM5/MPI-OM, run 2) have $R_\beta(z)$ values < 1.0 for trends in $T_{2\mathrm{LT}}$ and T_{Fu}. These anomalous results are due to either very weak surface warming (INM-CM3.0) or very weak surface cooling (ECHAM5/MPI-OM, run 2). Neither case is analogous to the radiosonde- or UAH-based $R_\beta(z) \ll 1.0$ results, which occur in conjunction with pronounced surface warming. The ECHAM result arises from the chance occurrence of a large La Niña event near the end of the 1979-1999 period. Run 1 of MRI-CGCM2.3.2 has very large $R_\beta(z)$ values, which are associated with T_S, $T_{2\mathrm{LT}}$, and T_{Fu} trends that are all close to

zero (Figs. 4C,D).

Caption for Figure S1

Figure S1: Scatter plots of the individual components of the $R_S(z)$ scaling ratio. Results are for the deep tropics (20°N-20°S). Panel **A** is identical to Fig. 4A, and provides information on the monthly-timescale variability in T_S and T_{2LT} in a wide range of model and observational datasets. The standard deviations of T_S and T_{2LT} in panel **B** are based on annual-mean rather than monthly-mean anomalies. All standard deviations were calculated from linearly detrended data. Observed $s\{T_S\}$ values are from NOAA (*S9*). The fitted regression lines (in red) are based on model data only. The black lines denote a slope of 1. For further details of datasets and analysis periods, refer to Fig. 4. Note the close correspondence between the monthly-mean and annual-mean results, which is due to the fact that monthly-timescale variability in T_S and T_{2LT} is dominated by interannual fluctuations in ENSO.

Supporting References and Notes

S1. B. D. Santer *et al.*, *J. Geophys. Res.* **104**, 6305 (1999).

S2. K. Y. Vinnikov, N. C. Grody, *Science* **302**, 269 (2003).

S3. Q. Fu and C. M. Johanson, *Geophys. Res. Lett.* **32**, L10703, doi:10.1029/2004GL022266 (2005).

S4. J. W. Hurrell, K. E. Trenberth, *J. Clim.* **11**, 945 (1998).

S5. V. Ramanathan *et al.*, *Proc. Nat. Acad. Sci.* **102**, doi: 10.1073/pnas.0500656102 (2005).

S6. V. Ramaswamy *et al.*, *Rev. Geophys.* **39**, 71 (2001).

S7. J. E. Hansen *et al.*, *J. Geophys. Res.* **107**, ACL-2, doi:10.1029/2001JD001143 (2002).

S8. L. Bengtsson, E. Roeckner, M. Stendel, *J. Geophys. Res.* **104**, 3865 (1999).

S9. T. M. Smith, R. W. Reynolds, *J. Clim.*, in press (2005).

Table 1: Forcings used in IPCC simulations of 20th century climate change

	Model	G	O	SD	SI	BC	OC	MD	SS	LU	SO	VL
1	CCCma-CGCM3.1(T47)	Y	-	Y	-	-	-	-	-	-	-	-
2	CCSM3	Y	Y	Y	-	Y	-	-	-	-	Y	Y
3	CNRM-CM3	Y	Y	Y	-	Y	?	-	-	-	-	-
4	CSIRO-Mk3.0	Y	-	Y	-	?	?	?	?	?	?	?
5	ECHAM5/MPI-OM	Y	Y	Y	Y	-	-	-	-	-	-	-
6	FGOALS-g1.0	Y	-	Y	?	-	-	-	-	-	-	-
7	GFDL-CM2.0	Y	Y	Y	-	Y	Y	-	-	Y	Y	Y
8	GFDL-CM2.1	Y	Y	Y	-	Y	Y	-	-	Y	Y	Y
9	GISS-AOM	Y	-	Y	-	-	-	-	Y	-	-	-
10	GISS-EH	Y	Y	Y	Y	Y	Y	Y	Y	Y	Y	Y
11	GISS-ER	Y	Y	Y	Y	Y	Y	Y	Y	Y	Y	Y
12	INM-CM3.0	Y	-	Y	-	-	-	-	-	-	Y	a
13	IPSL-CM4	Y	-	Y	?	-	-	-	-	-	-	-
14	MIROC3.2(medres)	Y	Y	Y	?	Y	Y	Y	Y	Y	Y	Y
15	MIROC3.2(hires)	Y	Y	Y	?	Y	Y	Y	Y	Y	Y	Y
16	MRI-CGCM2.3.2	Y	-	Y	-	-	-	-	-	-	Y	a
17	PCM	Y	Y	Y	-	-	-	-	-	-	Y	Y
18	UKMO-HadCM3	Y	Y	Y	Y	-	-	-	-	-	-	-
19	UKMO-HadGEM1	Y	Y	Y	Y	Y	Y	-	-	Y	Y	Y

G = Well-mixed greenhouse gases

O = Tropospheric and stratospheric ozone

SD = Sulfate aerosol direct effects

SI = Sulfate aerosol indirect effects

BC = Black carbon

OC = Organic carbon

MD = Mineral dust

SS = Sea salt

LU = Land use change

SO = Solar irradiance

VL = Volcanic aerosols.

a = Documentation claims inclusion of volcanic aerosols, but there are no stratospheric warming responses in T_4.

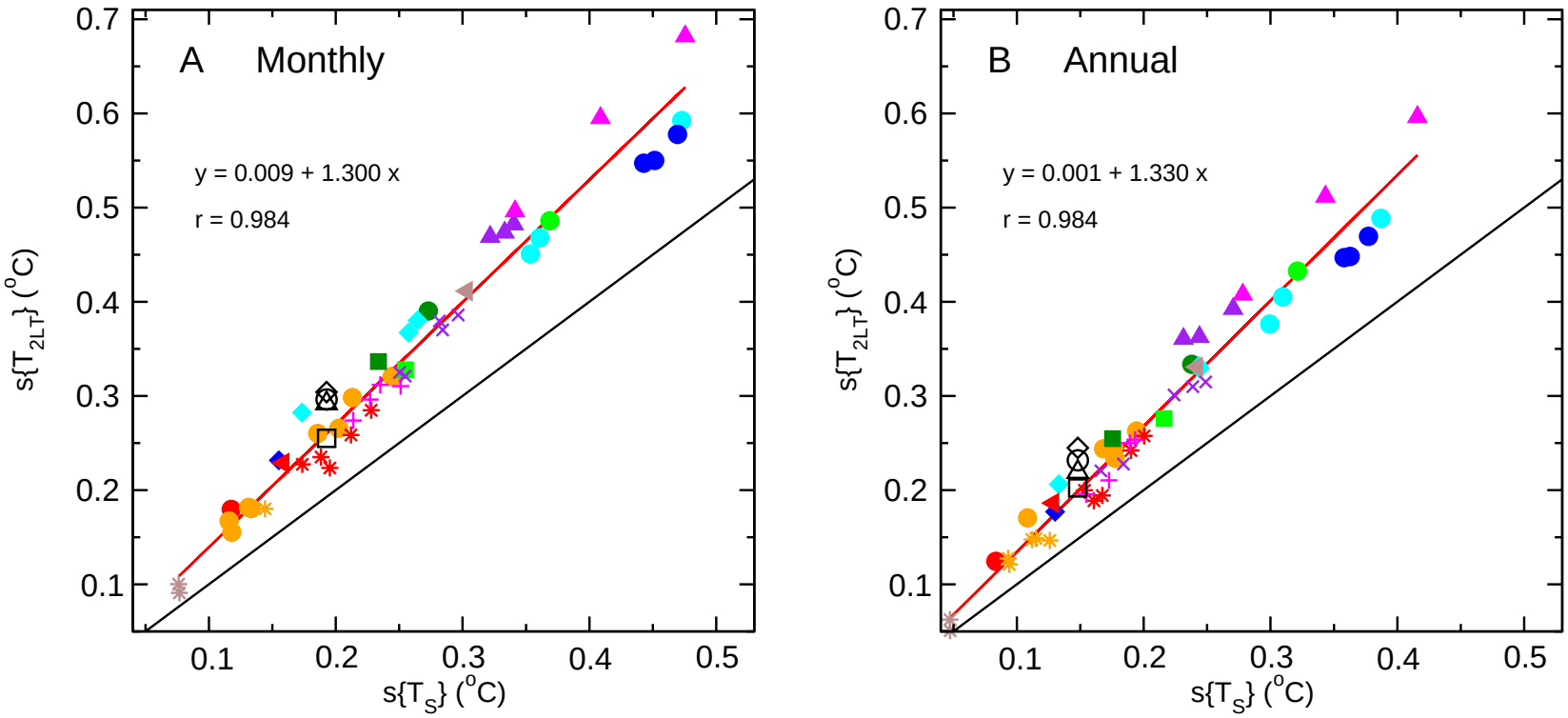

MODELS

- CCCma-CGCM3.1(T47)
- CCSM3
- CNRM-CM3
- CSIRO-Mk3.0
- ECHAM5/MPI-OM
- FGOALS-g1.0
- GFDL-CM2.0
- GFDL-CM2.1
- GISS-AOM
- GISS-EH
- GISS-ER
- INM-CM3.0
- IPSL-CM4
- MIROC3.2(medres)
- MIROC3.2(hires)
- MRI-CGCM2.3.2
- PCM
- UKMO-HadCM3
- UKMO-HadGEM1

OBSERVATIONS

- Radiosondes (RATPAC)
- Radiosondes (HadAT2)
- Satellites (UAH)
- Satellites (RSS)

Santer et al. Figure S1